Form and Function in Chinese Bound Foot

Qichang Mei (qmei907@aucklanduni.ac.nz)
Ningbo University https://orcid.org/0000-0003-1113-877X
yaodong gu
Ningbo University
Julie Kim
The University of Auckland
Liangliang Xiang
The University of Auckland
Vickie Shim
The University of Auckland
Justin Fernandez
The University of Auckland

Article

Keywords:

Posted Date: February 2nd, 2022

DOI: https://doi.org/10.21203/rs.3.rs-1311152/v1

Abstract

Foot adaptation in the typically developed foot is well explored. In this study, we explore the form and function in an atypical foot, the Chinese Bound foot. We evaluate the foot shape and posture, gait plantar loading and bone density adaptation. The atypical foot with binding practice led to increased foot arch and vertically oriented calcaneus. This causes the tibia, which typically acts as a load transfer beam and shock absorber to extend its function all the way through the talus to the calcaneus. This is evident in the bound foot by (i) reduced Center of pressure movement in the medial-lateral direction, suggesting reduced supination-pronation; (ii) increased density and stress in the talus-calcaneus articulation; and (iii) increased bone growth in the bound foot at articulation joints in the tibia, talus, and calcaneus. Knowledge may provide insights into the understanding of bone resorption and adaptation in response to different loading profiles.

Introduction

The Chinese Bound Foot, while not practised anymore, is a good example of an atypical foot form that demonstrates form and function. The human foot has evolved and adapted in its shape and function due to remodelling to adapt to the environment [1]. The Chinese Bound Foot, also known as 'Foot Binding', has its origins approximately between the late Tang dynasty and early Song dynasty [2]. This traditional custom has been practiced for over one thousand years, and was banned in the early 20th century [2,3]. The binding practice was performed in early childhood for girls at 5-7 years of age, by bending the toes (except the large toe) underneath the plantar surface and wrapping the metatarsals towards the calcaneus using bandages, which would be replaced throughout life, thus forming a significantly shortened foot and prominently high arch with realigned bony structures [4]. Although this practice was banned in the early 20th century, elderly females who lived in rural areas still continued to have their feet bound for some time after it was banned [5–9]. The Full Bound (FB) foot was defined as practicing foot binding throughout life, forming deformed toes and a high arch. The Half Bound (HB) foot was defined as practicing foot binding and releasing the binding since banning of the custom, also forming a deformed foot structure, particularly in the toes (Fig. 1).

The foot posture differences between the FB, HB and normal foot (NF) have been associated with reported differences in foot bone density. The shape characteristics of bound feet included an atypical high-arch in the midfoot, vertically oriented calcaneus, dislocated phalanges, and lower bone density as observed in X-ray and/or CT imaging studies [5,6,10]. However, the classification of foot binding type was not reported, as the half bound could only be found since banning this practice. While considering the binding practice [2,11], the toes (apart from the hallux) were flexed or curled underneath the plantar surface, which was believed to dislocate the phalanges from the metatarsals, thus losing the supporting function in the foot [12]. The binding force folded the metatarsals towards the calcaneus, leading to a vertically aligned calcaneus as an extension of the shank and talus. Foot binding led to reduced physical activity

and increased susceptibility to osteoporosis, but they did not have higher rates of fractures than typical feet likely due to compensation in activities and body balance [8].

Gait characteristics of females with bound feet have been reported including daily activities, such as walking [5,13,14]. Gait experiments indicated an increased cadence, decreased stride length, and decreased range of motion at the knee and ankle joints in bound foot females [15]. This was possibly related to the deformed forefoot (metatarsals), leading to restricted ankle rollover during stance and reduced range of motion. Studies of walking footprint and plantar pressure distribution revealed focalised pressure at the heel region [7,16] in the bound foot. From a functional perspective, the vertically oriented calcaneus was described as an extension of the lower leg for shock dampening [11], thus leading to the remodelling of the calcaneus [11]. Evidence of bound foot gait adapting to this foot condition has been reported [8]. Additional information including anthropometric, lifestyle questionnaires, calcaneus quantitative ultrasound and high-resolution peripheral quantitative CT (HR-qQCT) reported higher risks of osteoporosis in the calcaneus than healthy females [8]. In addition, the foot binding condition increased the risk of falling [5].

The objective of this study is to examine two versions of the Chinese Bound Foot, the FB and HB, and compare with a similarly aged typical female foot to demonstrate the form and function in human foot. To our knowledge this is the first-time gait, plantar pressure, bone shape analysis and finite element modelling have been integrated to evaluate the Chinese Bound Foot. The aim is to evaluate if foot plantar loading and foot posture can explain the adaptation in the bone shape and bone density.

Materials And Methods

Participants

Three female participants joined this study following ethical approval at Ningbo University. They were all elderly, and one exhibited a typical (normal) foot (NF), one was classified as half bound (HB) and the final participant had a full bound (FB) foot (see Table 1 for all demographics). They were informed of the objectives, requirements and procedures of this project and provided written consent.

Table 1
Demographics of participants

	Normal Foot	Half Bound	Full Bound
Age (yrs)	71	84	92
Height (m)	1.56	1.56	1.53
Mass (kg)	52.2	49.1	47.5
Foot Length (mm)	214.06	202.81	165.86
Foot Width (mm)	84.17	67.14	65.25

The complete framework for this study included segmentation of foot geometries for shape analysis and FE model construction for the NF, HB and FB. We then integrated foot plantar pressure to simulate internal bone stress and predicted bone remodelling adaptation. Fig. 2. highlights the steps and geometric models created for each stage of the computational pipeline.

Collection and Processing of Experimental Data

Participants attended the gait test and foot computed tomography (CT) scanning sessions separately. The gait test session collected walking kinematics and plantar pressure of both feet, part of which were reported in our previous work [15,16]. Three participants walked with a Pedar pressure system (Novel Pedar System, Germany) to record the plantar pressure at a frequency of 50Hz. Socks were worn to assist the fixation of the insole to the plantar surface. The plantar pressure from both feet were measured and averaged over three trials. The plantar pressure of the left foot from two consecutive steps were used in the current study.

The plantar surface was divided into separate regions including the Hallux, Other Toes, Medial Forefoot, Lateral Forefoot, Medial Midfoot, Lateral Midfoot, Medial Rearfoot and Lateral Rearfoot for the normal foot (NF) participant. The half bound (HB) foot was divided into regions of Hallux, Medial Forefoot, Lateral Forefoot, Medial Rearfoot and Lateral Rearfoot, and the full bound (FB) foot was divided into regions of Medial Forefoot, Lateral Forefoot, Medial Rearfoot and Lateral Rearfoot. This was done as the bound foot has distinctly different contact with the ground and we wanted to contrast similar anatomical regions.

We measured the discrete peak and mean plantar pressure values, the vertical ground reaction force and the center of pressure (CoP) trajectory, following our previously established protocol [17,18]. The CoP trajectory was categorized into the coordinate system of x-axis (medial-lateral) and y-axis (anterior-

posterior) as time-varying one-dimensional variables. The trajectories in the **x**-axis and **y**-axis were then normalized to the width and length of each subject-specific foot shape before performing statistics using the one-dimensional statistical parametric mapping (SPM1d) [19,20].

A total of six trials of left plantar pressure data were included in the statistical analysis, specifically the discrete values of mean and peak pressure in each anatomical region, and time-varying vertical ground reaction force and CoP trajectory in the medial-lateral (x-axis) and anterior-posterior (y-axis) directions. The one-way analysis of variance (ANOVA) was firstly performed to check significance among the NF, HB and FB, then the post hoc t-test was taken to analyze differences between each two feet (specifically, HB versus NF, FB versus NF, and FB versus HB). The significance level was set at $p < 0.05$.

Following the gait test, participants attended a CT scanning session in the local hospital with the approved ethics. The CT scanning of left and right feet were conducted using a SIEMENS Scanner (SIEMENS CT VA0 COAD, Munich, Germany) in a non-weight bearing and supine position. The parameters were set with a slice thickness of 0.6mm and pixel size of 0.521mm x 0.521mm, with all CT images exported as DICOM file for segmentation. The DICOM file of foot images were manually segmented in the Mimics 21.0 (Materialise, Leuven, Belgium) (Fig. 2.). Before exporting as separate geometrical (stl) parts, the bone and tissue geometries were firstly smoothed with a smooth factor of 0.4, and then wrapped to eliminate geometric gaps of less than 0.7mm. The quality of each geometrical bone shape was checked using HyperMesh (2017, Altair, Troy, MI, USA) to ensure that the Jacobian of each element was greater than 0.3.

For bone shape comparison, the surface mesh (.stl) of the calcaneus, talus, tibia, fibula, tarsus (navicular, cuboid, medial/intermediate/lateral cuneiform), and 1-5 metatarsals bones were organized into a vector matrix. Following a previous established framework of statistical shape modelling (SSM)[21] using the musculoskeletal modelling software Gias2 (https://pypi.org/project/gias2/) developed at the Auckland Bioengineering Institute, a comparison of the shape of the HB, FB and NF was performed. This involved ensuring the HB, FB and NF had a consistent mesh topology using iterative closest point and partial least squares fitting [22–24], and centroid alignment [21,24–26]. The difference in bone shape was plotted using error maps with the opensource software CloudCompare (http://www.danielgm.net/cc/).

Development of Computational Finite Element Foot Model

The foot bones and skin mesh were exported from Mimics as stl files. The geometries were post-processed in Geomagic Studio 12 (Research Triangle Park, NC, United States) to diagnose ill conditioned elements and repair, then exported as surface files (iges) for meshing in HyperMesh 2017 (Altair Engineering Inc., Hyperworks, United States). Solid tetrahedral elements were then generated with element size of 2.0mm for bones and 3.0mm for soft tissue. All meshes were quality checked before exporting as inp files for model assembly in Abaqus (Dassault Systems Simulia Corp., Johnston, USA). These geometry sizes also provided mesh convergence for the Von Mises stress we were computing.

The bony structures were defined as linearly elastic isotropic materials with Young's Modulus of 7300MPa and Poisson's Ratio of 0.3 [27], and the lumped soft tissue encapsulating the bone was assigned with a linear elastic model (Young's modulus of 0.15MPa, Poisson's ratio of 0.45)[27]. The tibia and fibula proximal surface were fixed as boundary conditions for a quasi-static simulation and the plantar pressure was applied to the plantar surface of the foot mesh. Five linearly elastic connectors with stiffness of 200N/mm were created to link the calcaneus notch with the base of the proximal phalanges [28,29] to represent the plantar fascia. Five sets of rigid connector forces with a value assigned to 0.5BW were applied to the Achilles tendon representing calf muscles during gait [30].

The bone remodelling algorithm used is this study was adapted from Doblaré and García [31]. Macroscopic apparent bone density is predicted based on the principles of continuum damage mechanics. This model has been shown to give anatomically and biologically realistic bone adaptation predictions in the proximal femur. Readers are referred to Doblaré and García [31], but the basic implementation in our Abaqus model is presented in Appendix A below.

Results

Gait Performance

Figure 3**(a)** depicted the peak pressure distribution in the NF, HB, and FB foot. As included in the Fig. 1S, the overall distribution of mean plantar pressure (left) and peak plantar pressure (right) during stance are presented.

For the other toes (toes except hallux), the NF has high pressure while no pressure is exhibited in HB and FB feet. Similarly for the midfoot, the NF presents high pressure while no pressure is observed in HB and FB feet. Following an ANOVA and post hoc statistical analysis, the HB foot exhibited greater mean pressure ($p = 0.043$) and peak pressure ($p = 0.0244$) in the Hallux compared with the NF, whereas no pressure is observed in the FB hallux. In the forefoot, the NF presented higher mean pressure in the lateral forefoot than HB ($p = 0.0002 < 0.001$) and FB ($p = 0.01$) feet, and FB had higher mean pressure over HB ($p = 0.00025 < 0.001$). As for the peak pressure, NF and FB feet presented larger pressure than HB in both the medial ($p = 0.017$, $p = 0.00$) and lateral ($p = 0.0095 < 0.001$, $p = 0.00123 < 0.001$) forefoot. In the rearfoot, the mean pressures were similar across all three feet types, apart from the FB presenting smaller mean pressure than HB ($p = 0.00234 < 0.001$).

However, the FB showed significantly higher peak pressure than both the NF and HB. We used the mean pressure in each plantar region during stance as the boundary condition for the FE foot model. This is because the peak pressure typically resembled a small anatomical region and/or small time point during gait, which is less representative of the whole gait cycle.

Figure 3**(b)** presents the vertical ground reaction force during stance for all 3 feet. The NF participant presented a typical pattern of vertical ground reaction force with the first peak of weight acceptance and

second peak of push off. The difference in HB and FB differed significantly during the 30-40% of stance phase. The difference between HB and NF, and FB and NF were observed at the second peak of push-off, specifically with an atypical pushing-off during the 72-92% (FB vs NF) and 74-92% (HB vs NF) phases of stance. The details of comparison using SPM one-way ANOVA and the SPM post hoc t-test are presented are included in the **Fig. S2** and **Fig. S3**.

The centre of pressure (CoP) trajectory was explored for the NF, HB and FB foot. Fig. 4a shows during gait the CoP trajectory starts at the heel and migrates towards the medial forefoot for both the NF and HB, whereas the CoP migrates towards the lateral forefoot for the FB.

The medio-lateral CoP pathway (as a percentage of foot width) and anterior-posterior CoP pathway (as a percentage of foot length) were further explored to better understand foot balance. Fig. 4b **(left)** shows the medio-lateral CoP trajectory, and differences among the NF, HB and FB foot were observed in late stance, during the push-off phase, with greatest variation in the forefoot region. Specifically, the differences were observed in the 94-100% phase of stance (HB and NF), 80-100% phase of stance (FB and NF), and 76-100% phase of stance (FB and HB). Fig. 4b **(right)** shows the anterior-posterior CoP trajectory differences among the NF, HB and FB foot were also observed in late stance. Specifically, the differences were observed in the 92-100% phase of stance (HB and NF), 76-84% phase of stance (FB and NF), and 94-100% phase of stance (FB and HB).

Geometric and Shape Differences

The foot profiles (length and width) of the 3 elderly females are shown in the present study **(**Fig. 1**)**. Specifically, the measured lengths and widths were 214.06mm and 84.17mm for the NF, 202.81mm and 67.14mm for the HB foot, and 165.86mm and 65.25mm for the FB foot, respectively.

Hence, as expected, the HB and FB feet exhibited shorter lengths due to the foot binding compared to the NF. Moreover, the FB exhibited a high arch in the midfoot forming an extreme dome, compared to the HB and NF. The HB also showed a higher arch compared to the NF.

To further elucidate the 3D shape differences in the foot bones, we morphed the FB and HB geometric bones (tibia, fibula calcaneus, talus, 1-5 metatarsals) onto the NF as a reference. Fig. 5. shows that in general the HB and FB feet had smaller metatarsals than the NF, but the HB was larger than FB. The HB and FB fibula was also similar is size but smaller than the NF. Full details of the shapes are presented in the **Fig. S6.** (calcaneus), **Fig. S7.** (talus), **Fig. S8.** (tibia), **Fig. S9.** (fibula), **Fig. S10.** (M1), **Fig. S11.** (M2), **Fig. S12.** (M3), **Fig. S13.** (M4), **Fig. S14.** (M5), with quantification of Huasdorff Distance and Gaussian Distribution of the distances.

The tibia, talus and calcaneus were the main bones presenting differences. The HB tibia, talus and calcaneus presented larger features by 3-5mm than the NF, whereas the FB was smaller than the NF by 3-5mm. Specifically, the larger bone growth in the HB was observed primarily at the tibia-talus and talus-calcaneus articulations. As shown the Fig. 6., the regional shape variations in vertices of calcaneus, talus,

and tibia bones (hindfoot region) were quantified for illustration of the middle talar articular surface (calcaneus), posterior calcaneal articular surface (talus), and distal articular surface (tibia).

Finite Element simulations and CT validation

Figure 7. presents the von Mises (VM) bone stress distributions in the NF, HB and FB models from the Finite Element simulations of the stance phase of gait. The stress ranges from a low 0.4MPa in non-directly loaded regions, up to 5MPa in highly stressed regions. There are a few minor regions that experience loads up to 30MPa near bone articulations. It is observed that the NF has a more uniform stress distribution up to the metatarsals (with a slight peak on M5) relative to the HB and FB. The HB shows greater peak VM stress in the 1st metatarsal and hallux, with peak VM stress evident in the midfoot and talus. In contrast, the FB has high concentrated VM stress in the midfoot, with peak stresses in the calcaneus. Importantly, both the HB and FB do not show a uniform stress in the calcaneus compared with the NF.

Figure 8. presents the (**a**) FE predicted von Mises stress for stance, (**b**) predicted bone remodelling adaptation, and (**c**) CT slice with relative Hounsfield units for the calcaneus in the NF (i), HB (ii) and FB (iii) feet. Note that white regions represent cortical bone in the CT image, and grey regions represent lumped trabecular bone.

In the NF (Fig. 8i) the FE model predicted a consistent intensity of increased VM stress in the outer cortical region with peaks (~7.6 MPa) at the posterior Achilles tendon insert and anterior region articulating with the navicular bone. However, there was a low stress region observed near the superior surface articulating with the talus. This was consistent with 60 days of predicted bone remodelling showing increased thickening of bone density in the regions with higher VM stress. Comparison with the CT slice of the same specimen showed CT evidence of cortical bone uniformly around the outer edge with thicker bone at the Achilles tendon insert. However, at the talus-calcaneus articulation there is also CT evidence of cortical bone in contrast to the FE model prediction.

In the HB (**Fig. 8**ii) the FE model predicted a sparse VM stress in the outer cortical region with peaks (~2 MPa) at the posterior Achilles tendon insert and superior region articulating with the talus bone. The magnitude and intensity of the VM stress is much less than the NF. This was consistent with 60 days of predicted bone remodelling showing increased thickening of bone density primarily at the talus articulation. Comparison with the CT slice of the same specimen showed CT evidence of a thin cortical bone layer with increased density at the Achilles tendon inserts and talus articulation.

In the FB (**Fig. 8**iii) the FE model predicted a sparse VM stress in the outer cortical region with peaks (~7.6 MPa) at the posterior Achilles tendon insert and superior region articulating with the talus bone. The magnitude of the peaks was consistent with the NF but similar in pattern to the HB with peaks at bony articulation and tendon inserts. This was consistent with 60 days of predicted bone remodelling showing increased thickening of bone density primarily at the Achilles tendon insert and talus articulation. Comparison with the CT slice of the same specimen showed CT evidence of a thin cortical bone layer

with increased density at the Achilles tendon insert and increased density of trabecular structures at the talus articulation.

Discussion

A few considerations should be taken into account while acknowledging findings from the current study. Firstly, we only included a single representative of a NF, HB and FB female participant. These elderly females with half and full bound characteristics are the last generation, as this custom has been banned over a century ago, making it difficult to increase the sample size. It was rare to find and obtain all the information for the current participants. Secondly, the CT imaging data were acquired from a non-weight bearing position, which might not be the real geometrical condition during gait or other activities. However, we employed subject-specific foot shape, boundary conditions and external loadings all from the same subjects. Lastly, the material properties assigned were macroscopic models using simplified linear elastic material properties as it was not possible to obtain bone properties for each participant as the CT was not taken using a CT phantom. We were primarily interested in the relative pattern of bone density for model evaluation and plotted the relative Hounsfield instead.

Our models showed bound feet were shorter than typical feet due to bounding constraints and this was consistent with other studies. For example, Qin et al. [8] reported average lengths of 223mm in bound feet and 254mm for typical feet, and Reischl et al. [7] reported a length of 18cm for bound foot and 22cm for typical feet. This shorter length is associated with compressed bones and a higher arch in the bound foot. Specifically, the extreme dome-like arch in the FB formed due to the vertically re-oriented calcaneus and metatarsals following lifelong foot binding constraints. Whereas the HB presented only deformed toes since the binding was released earlier in age giving the foot bones an opportunity to grow with a small foot arch. Our model findings were consistent with previous studies that analysed the bone re-alignment in bound feet. Specifically, increased horizontal metatarsals angle comparing to the NF [32], increased bending and rotational articulation between the calcaneus and metatarsals in the BF [4] and vertical orientation of BF calcaneus [5,6,10,33].

Our statistical mapping of the FB and HB bones onto the NF revealed size and shape differences. We found that in general the bones were smaller in the forefoot (especially the metatarsals) and this was consistent with the lower mean and peak plantar pressure that the HB and FB feet experience due to binding. Recent paleopathology studies [13,34,35] found a similar finding by comparing recovered bound foot remains to the bones in the normal foot. Macroscopic examination of the shapes reported that the metatarsals (particularly 2-5) reduced in length and presented thin, gracile shafts and small distal heads. Interestingly, they found that M1 was not always smaller and this is consistent with our finding for M1, which showed increased FE stress relative to the other metartarsals, and was also slightly larger at the ends, especially in the HB foot. Shape differences in the rearfoot exhibited more adaption due to form and function of loading absoprtion. In particular, we found that the articulating joint surfaces in the HB and FB had greater variation in size than the NF. While there are few studies analysing bone shape in the

bound foot we did identify one study that showed the talus of bound feet have extended and flattened articular joint surfaces [13,35], consistent with our work. Further, the calcaneal sulcus in the HB and FB were larger than the NF, and the likely functional reason for this alteration is the articulation with the talus must be a more stable joint as the rearfoot bears most loading during walking in the bound foot (HB and FB). Moreover, the increased size of the tibia and talus articulation supports this idea. It is as if the function of the tibia as a vertical load bearing beam is extended down to the calcaneus.

The toe plantar pressure is relatively small in the HB and NF and there is no midfoot loading due to compromised structural support. However, the plantar pressure pattern is more focussed towards the rear with increased bound contraints. For example, in our model the NF is fairly even in pressure between the rearfoot, midfoot, forefoot and toes. However, the HB foot is focussed on the rearfoot, reduced on the forefoot and only the hallux, whereas the FB is solely focussed on the rearfoot and forefoot. This focus towards the rear of the foot is consistent with the idea that the rearfoot is an extension of the lower extremity for shock dampening in the Chinese bound foot [7,11,16]. Furthermore, the reduced mean plantar pressure at the rear in the HB and FB are consistent with the reduced ground reaction forces we found during the push-off phase of gait. This is consistent with the deformity in the forefoot and toes affecting the natural ankle roll-over motion during gait, providing limited ankle range of motion in the sagittal plane during stance [16].

We did not observe major differences in the CoP for the bound foot participants versus the NF except during the push-off phase. The CoP path from rear to hallux was consistent with normal walking [7] although slightly more lateral, which is consistent with a recent report that CoP trajectory shifts laterally in old age [36]. The primary difference was observed in the FB, where the CoP moved more laterally during push-off, which was not observed in the HB as the hallux was still articulating in the HB foot. It was also observed in the FB that the medial-lateral CoP only varied within 10% of the foot width. This suggest that the FB had limited supination-pronation motion, which was not observed in the HB foot. Furthermore, the anterior-posterior CoP of the FB foot occupied only 20% of the foot length for 70% of stance unlike the HB and NF. These two CoP patterns suggest that the rearfoot took most of the loading in the FB foot and implies that the FB foot is functioning more like a rigid shock mechanism.

The calcaneus was investigated for its function as a posterior balance support and shock absorption mechanism. We observed in the NF that the VM stress and predicted bone density was consistent around the cortical shell and higher at the Achilles tendon insert and joint articulation. We found that this was consistent with the CT evidence of relative Hounsfield data from that same subject, however, our model did not predict density at one aspect of the talus articulation. We attribute this to the fact that our model was limited to only looking at one pose of the foot (built from CT), which was loaded with the mean plantar pressure from stance. We did not consider the dynamic articulation of the joint that would have provided a complete loading from gait and loaded the calcaneus fully from different orientations. However, we suggest from our results that a static simple model using mean pressure from gait reveals a good prediction of bone adaptation without the need to consider other tasks. Our prediction of the HB and

FB feet improved our confidence in our approach as it predicted a thin bone density along the cortical shell and increased density only at the talus articulation and Achilles tendon insertion site. The CT evidence for both revealed a thinner bone density along the shell and increased density and/or trabecular density at the same anatomical region as the model. The increased VM stress and bone density which moved progressively posterior was consistent with the increasing vertical orientation of the calcaneus from the HB to the FB foot. This was also consistent with a recent study that found considerable loss of trabecular density in the calcanues bones of bound feet [34], however, the trabecular anistropy in the calcaneus of bound foot typically remains unchanged [11]. While we did not characterise the anisotropy in our study we did note that the trabecular lines still remain consistent across all 3 models even though the density has been reduced. This suggests that the underlying loading patterns of principal stress are still similar.

In summary, this study is the first investigation to the author's knowledge of form and function in the Chinese Bound foot combing gait, shape analysis and computational stress and bone density prediction., this study has revealed an insightful form and function finding through considering an atypical foot model. When the foot is bound the foot arch increases and the calcaneus orients vertically. This causes the tibia, which typically acts as a load transfer beam and shock absorber to extend its function all the way through the talus to the calcaneus. This is evident in the bound foot by (**i**) reduced CoP movement in the medial-lateral direction, which suggests reduced supination-pronatation; (**ii**) increased density and stress in the talus-calcaneus articulation; and (**iii**) increased bone growth in the bound foot at articulation joints in the tibia, talus and calcaneus.

Declarations

Acknowledgments

QM of this paper was supported by the New Zealand-China Doctoral Research Scholarship issued from the Ministry of Foreign Affairs and Trade (New Zealand) and China Scholarship Council (CSC). LX is currently supported by the China Scholarship Council (CSC). Authors would like to thank the family of the elderly females for the kind cooperation during the data collection.

Funding: This study was sponsored by the following fundings bodies:

National Natural Science Foundation of China (No.81772423);

NSFC (Natural Science Foundation of China) - RSE (The Royal Society of Edinburgh) Joint Project (No. 81911530253);

and K. C. Wong Magna Fund in Ningbo University.

Author contributions: Conceptualization: QM, YG, JF; Methodology: QM, JK, VS; Investigation: QM, YG, JK, LX; Visualization: QM, JK; Supervision: YG, JF; Writing—original draft: QM, JF; Writing review & editing: QM, YG, VS, JF

Competing interests: Authors declare that they have no competing interests.

Data and materials availability: All data are available in the main text or the supplementary materials.

Supplementary Text

Fig. S1. Overall plantar pressure distribution and discrete pressures in each plantar region.

Fig. S2. The comparison of vertical ground reaction force using SPM one-way analysis of variance (ANOVA) and post hoc t test.

Fig. S3. The comparison of Med-Lat CoP trajectory using SPM one-way analysis of variance (ANOVA) and post hoc t-test.

Fig. S4. The comparison of Ant-Post CoP trajectory using SPM one-way analysis of variance (ANOVA) and post hoc t-test.

Fig. S5. Illustration of the Center of Pressure trajectory in the Normal Foot, Half-Bound and Foot-Bound Feet during gait.

Fig. S6. Illustration of shape differences in the calcaneus bone of HB and NF, and FB and NF with quantification of Hausdorff Distance, and Gaussian Distribution.

Fig. S7. Illustration of shape differences in the talus bone of HB and NF, and FB and NF with quantification of Hausdorff Distance, and Gaussian Distribution.

Fig. S8. Illustration of shape differences in the tibia bone of HB and NF, and FB and NF with quantification of Hausdorff Distance, and Gaussian Distribution.

Fig. S9. Illustration of shape differences in the fibula bone of HB and NF, and FB and NF with quantification of Hausdorff Distance, and Gaussian Distribution.

Fig. S10. Illustration of shape differences in the M1 bone of HB and NF, and FB and NF with quantification of Hausdorff Distance, and Gaussian Distribution.

Fig. S11. Illustration of shape differences in the M2 bone of HB and NF, and FB and NF with quantification of Hausdorff Distance, and Gaussian Distribution.

Fig. S12. Illustration of shape differences in the M3 bone of HB and NF, and FB and NF with quantification of Hausdorff Distance, and Gaussian Distribution.

Fig. S13. Illustration of shape differences in the M4 bone of HB and NF, and FB and NF with quantification of Hausdorff Distance, and Gaussian Distribution.

Fig. S14. Illustration of shape differences in the M5 bone of HB and NF, and FB and NF with quantification of Hausdorff Distance, and Gaussian Distribution.

References

1. Ambrosi, D. *et al.* Growth and remodelling of living tissues: Perspectives, challenges and opportunities. J. R. Soc. Interface **16**, 20190233 (2019).
2. Greenhalgh, S. Bound Feet, Hobbled Lives: Women in Old China. Front. A J. Women Stud. **2**, 7–21 (1977).
3. Jackson, R. The Chinese Foot-Binding Syndrome: Observations on the History and Sequelae of Wearing Ill-Fitting Shoes. Int. J. Dermatol. **29**, 322–328 (1990).
4. Stone, P. K. Binding women: Ethnology, skeletal deformations, and violence against women. Int. J. Paleopathol. **2**, 53–60 (2012).
5. Richardson, M. L. Chinese Foot Binding: Radiographic Findings and Case Report. Radiol. Case Reports **4**, 270 (2009).
6. Gu, Y., Li, J. & Li, Z. Deformation of Female Foot Binding in China. J. Clin. Rheumatol. **19**, 418 (2013).
7. Reischl, U., Nandikolla, V., Colby, C., Mijović, B. & Wei, H. C. A case study of Chinese bound feet: Application of footprint analysis. Coll. Antropol. **32**, 629–632 (2008).
8. Qin, L. *et al.* Lifelong bound feet in China: A quantitative ultrasound and lifestyle questionnaire study in postmenopausal women. BMJ Open **5**, e006521 (2015).
9. Pan, Y. *et al.* A study on bone mass in elderly Chinese foot-binding women. *Int. J. Endocrinol.* 2013, 351670 (2013).
10. Munk, P. L. & Poon, P. Y. Bound feet in an elderly Chinese woman. Am. J. Roentgenol. **167**, 1216 (1996).
11. Reznikov, N. *et al.* Functional Adaptation of the Calcaneus in Historical Foot Binding. J. Bone Miner. Res. **32**, 1915–1925 (2017).
12. Lambrinudi, C. Use and Abuse of Toes. Postgrad. Med. J. **8**, 459–464 (1932).
13. Lee, C. A bioarchaeological and biocultural investigation of Chinese footbinding at the Xuecun archaeological site, Henan Province, China. Int. J. Paleopathol. **25**, 9–19 (2019).

14. Cummings, S. R., Ling, X. & Stone, K. Consequences of Foot Binding among older women in Beijing, China. Am. J. Public Health **87**, 1677–1679 (1997).
15. Zhang, Y., Feng, N., Hu, N. & Gu, Y. A pilot study on gait kinematics of old women with bound feet. *Appl. Bionics Biomech.* 2015, 589709 (2015).
16. Gu, Y. *et al.* Foot loading characteristics of Chinese bound feet women: A comparative analysis. PLoS One **10**, e0121695 (2015).
17. Mei, Q., Feng, N., Ren, X. J. X., Lake, M. & Gu, Y. D. Y. Y. D. Foot Loading Patterns With Different Unstable Soles Structure. J. Mech. Med. Biol. **15**, 1550014 (2015).
18. Mei, Q., Gu, Y. & Fernandez, J. Alterations of Pregnant Gait during Pregnancy and Post-Partum. Sci. Rep. **8**, 2217 (2018).
19. Pataky, T. C. *et al.* Vector field statistics for objective center-of-pressure trajectory analysis during gait, with evidence of scalar sensitivity to small coordinate system rotations. Gait Posture **40**, 255–258 (2014).
20. Booth, B. G., Keijsers, N. L. W., Sijbers, J. & Huysmans, T. STAPP: Spatiotemporal analysis of plantar pressure measurements using statistical parametric mapping. *Gait Posture* **63**, 268–275 (2018).
21. Zhang, J., Malcolm, D., Hislop-Jambrich, J., Thomas, C. D. L. & Nielsen, P. M. F. An anatomical region-based statistical shape model of the human femur. Comput. Methods Biomech. Biomed. Eng. Imaging Vis. **2**, 176–185 (2014).
22. Sarkalkan, N., Weinans, H. & Zadpoor, A. A. Statistical shape and appearance models of bones. Bone **60**, 129–140 (2014).
23. Besl, P. J. & McKay, N. D. A Method for Registration of 3-D Shapes. IEEE Trans. Pattern Anal. Mach. Intell. **14**, 239–256 (1992).
24. Zhang, J., Hislop-Jambrich, J. & Besier, T. F. Predictive statistical models of baseline variations in 3-D femoral cortex morphology. Med. Eng. Phys. **38**, 450–457 (2016).
25. Mei, Q., Gao, Z., Fernandez, J. & Gu, Y. 3D Foot Shape Modelling Based on Statistical Shape Model. J. Med. Biomech. **36**, 96–101 (2021).
26. Xiang, L. *et al.* Evaluating Function in the Hallux Valgus Foot Following a 12-week Minimalist Footwear Intervention: A Pilot Computational Analysis. J. Biomech. **132**, 110941 (2022).
27. Cheung, J. T. M. & Zhang, M. A 3-dimensional finite element model of the human foot and ankle for insole design. Arch. Phys. Med. Rehabil. **86**, 353–358 (2005).
28. Chen, T. L. W., Wong, D. W. C., Wang, Y., Lin, J. & Zhang, M. Foot arch deformation and plantar fascia loading during running with rearfoot strike and forefoot strike: A dynamic finite element analysis. J. Biomech. **83**, 260–272 (2019).
29. Kitaoka, H. B., Luo, Z. P., An, K. N., Growney, E. S. & Berglund, L. J. Material Properties of the Plantar Aponeurosis. Foot Ankle Int. **15**, 557–560 (1994).
30. Cheung, T.-M. J., Zhang, M. & An, K. N. Effects of plantar fascia stiffness on the biomechanical responses of the ankle-foot complex. Clin. Biomech. **19**, 839–846 (2004).

31. Doblaré, M. & García, J. M. Anisotropic bone remodelling model based on a continuum damage-repair theory. J. Biomech. **35**, 1–17 (2002).
32. Ma, J., Song, Y., Rong, M. & Gu, Y. Bound foot metatarsals skeletal rays kinematics information through inverse modelling. Int. J. Biomed. Eng. Technol. **13**, 147–153 (2013).
33. Howard, R. & Pillinger, M. H. Consequences of Chinese foot binding. J. Clin. Rheumatol. **16**, 408 (2010).
34. Zhao, Y. *et al.* Osteological characteristics of Chinese foot-binding in archaeological remains. Int. J. Paleopathol. **28**, 48–58 (2020).
35. Berger, E., Yang, L. & Ye, W. Foot binding in a Ming dynasty cemetery near Xi'an, China. Int. J. Paleopathol. **24**, 79–88 (2019).
36. Sole, G., Pataky, T., Sole, C. C., Hale, L. & Milosavljevic, S. Age-related plantar centre of pressure trajectory changes during barefoot walking. Gait Posture **57**, 188–192 (2017).

Figures

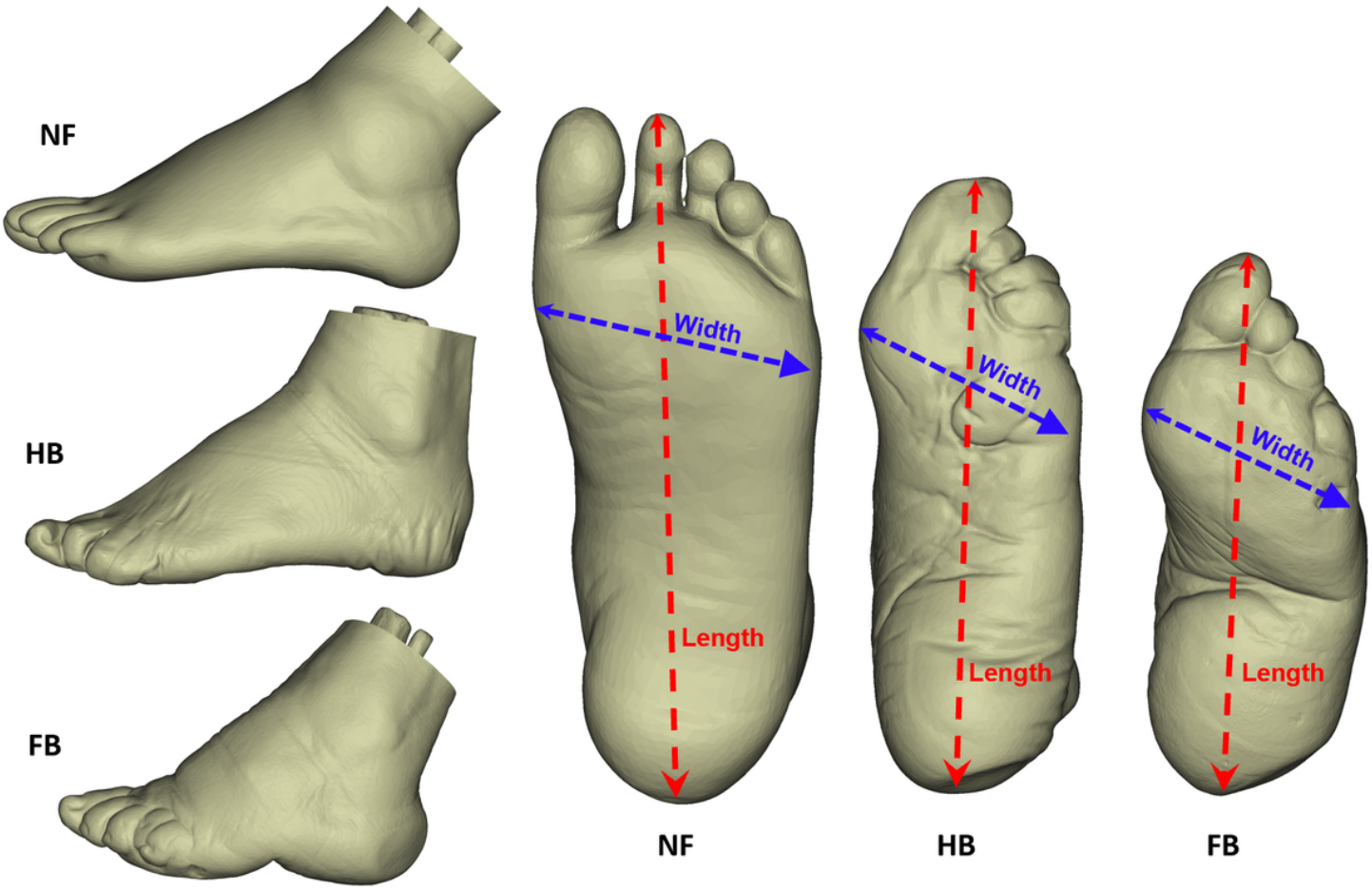

Figure 1

Lateral and plantar view of Normal Foot (NF), Half Bound (HB) and Full Bound (FB) foot

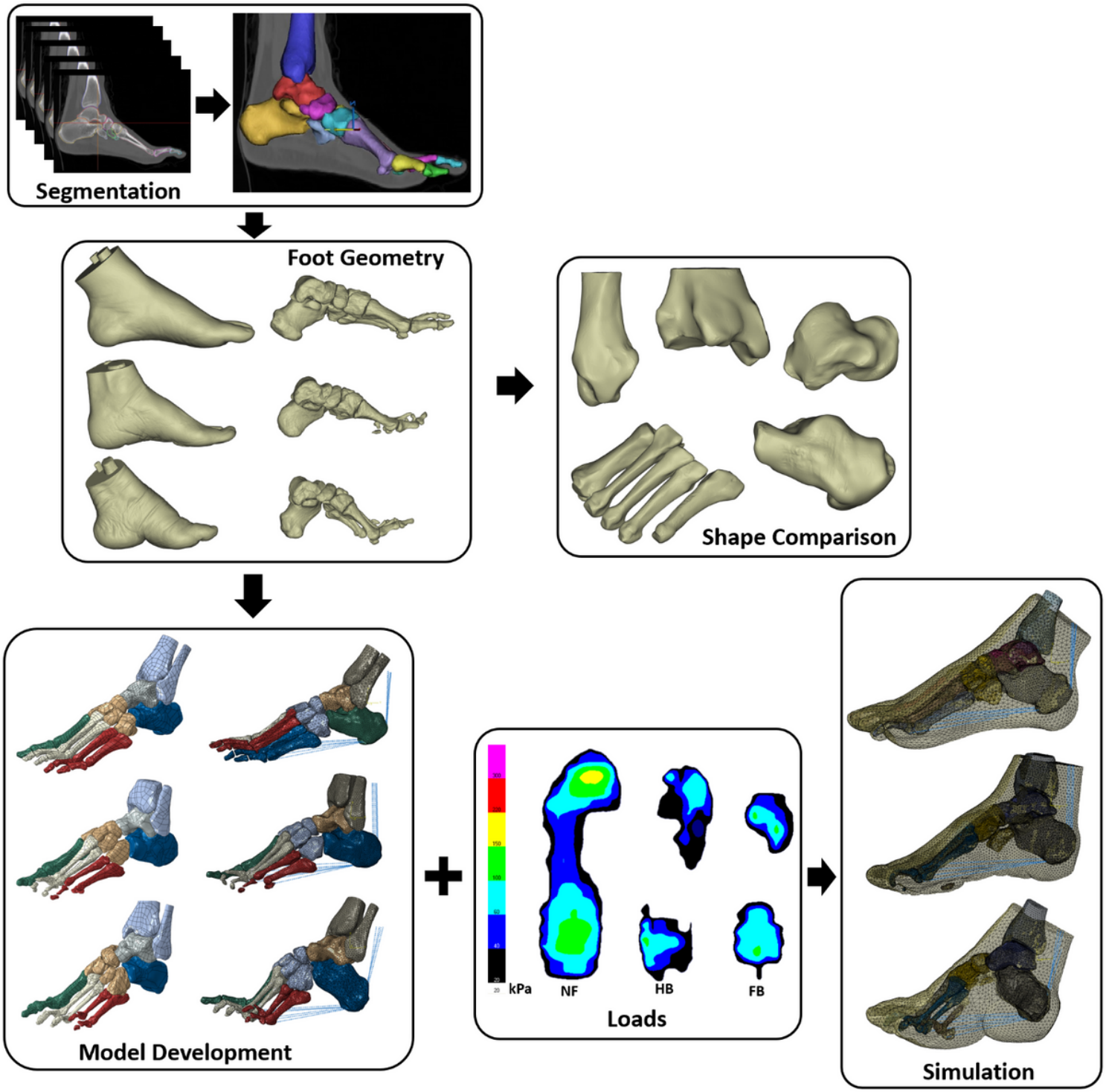

Figure 2

Framework of segmentation, shape comparison, FE model development and simulation.

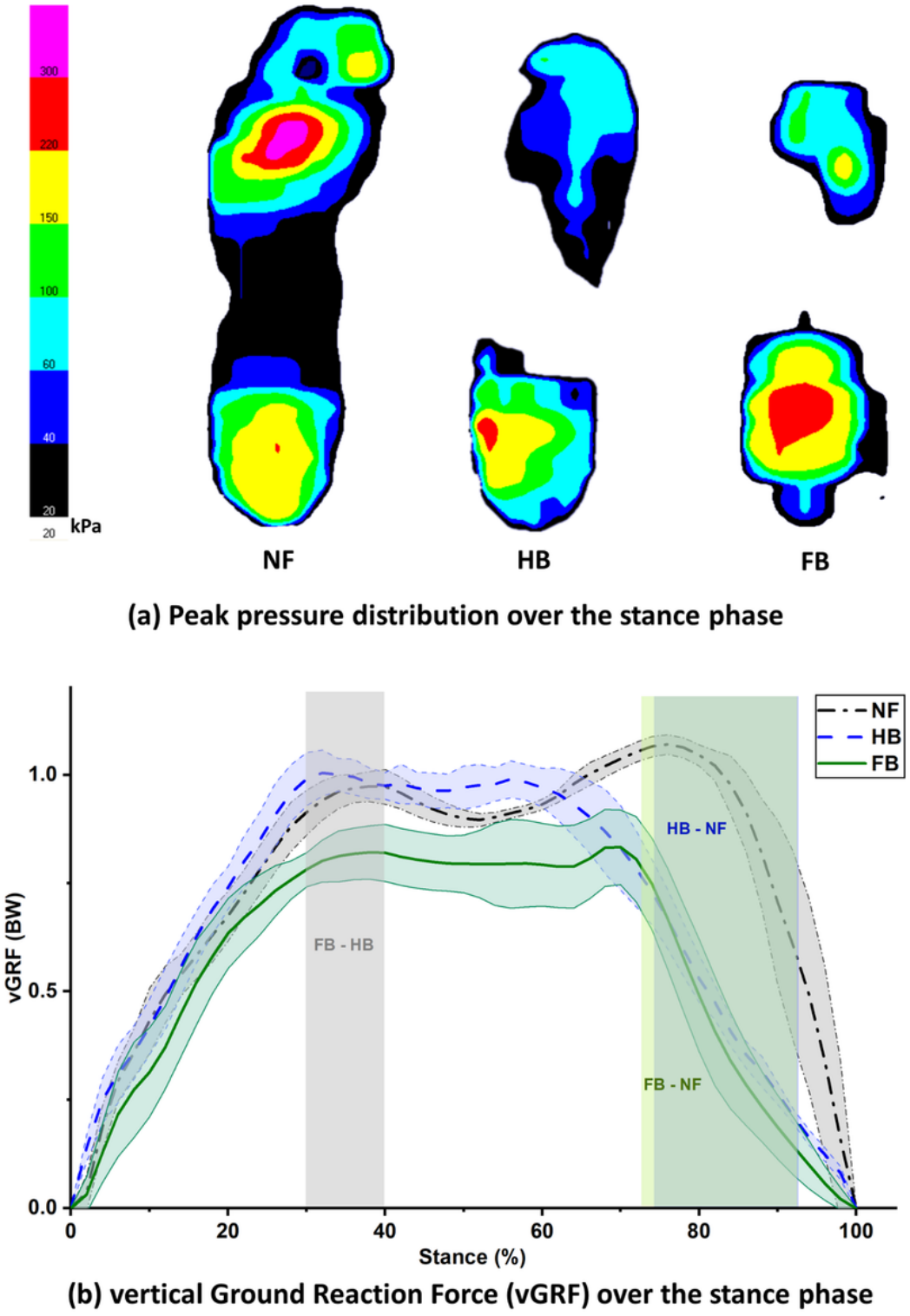

Figure 3

The peak pressure distribution during stance (**a**) and vertical ground reaction force (**b**) in the NF, HB, and FB foot types.

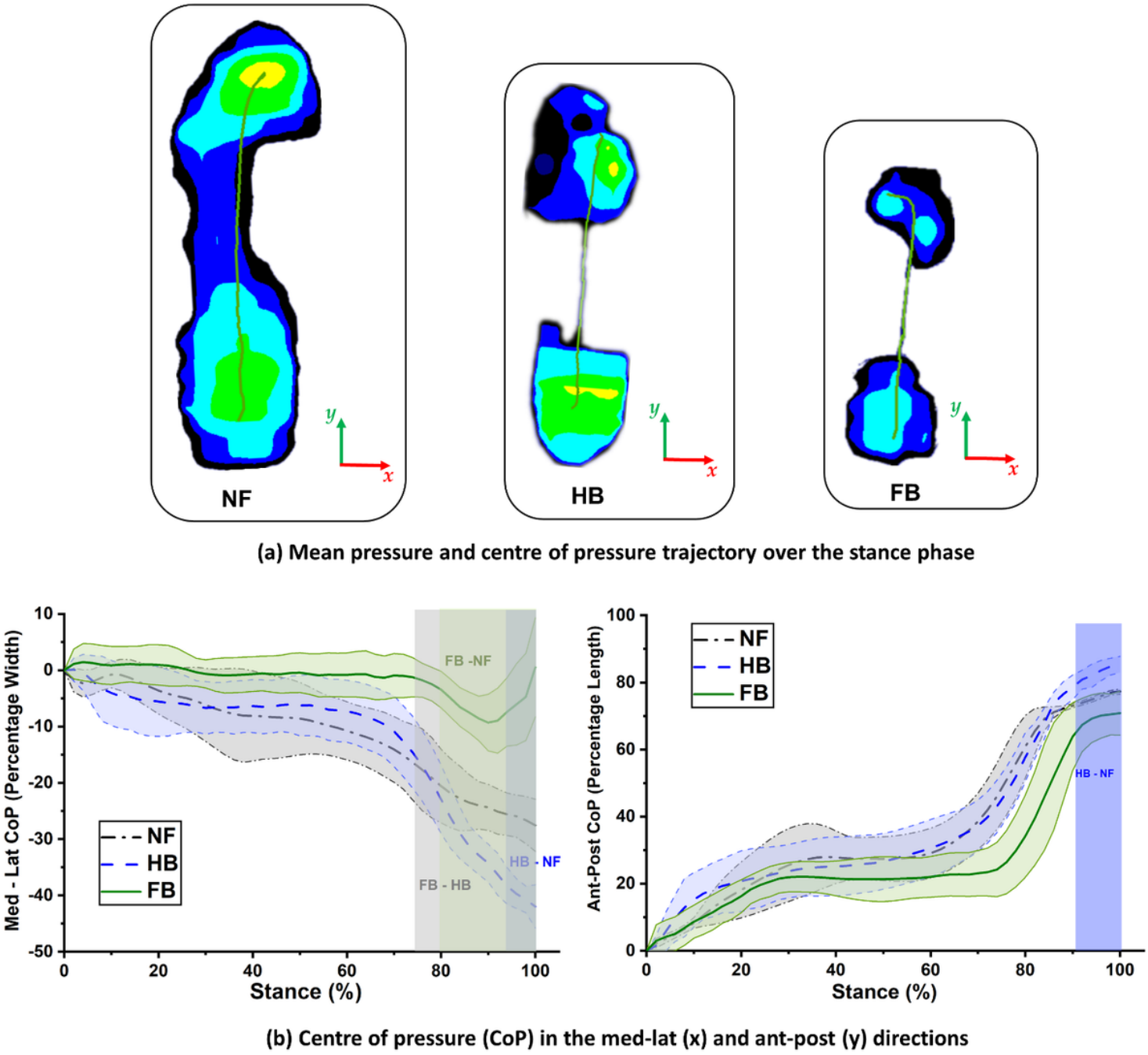

Figure 4

Center of Pressure trajectory in the NF, HB and FB foot during stance (**a**) and comparison of Med-Lat (left) and Ant-Post (right) CoP trajectories (**b**).

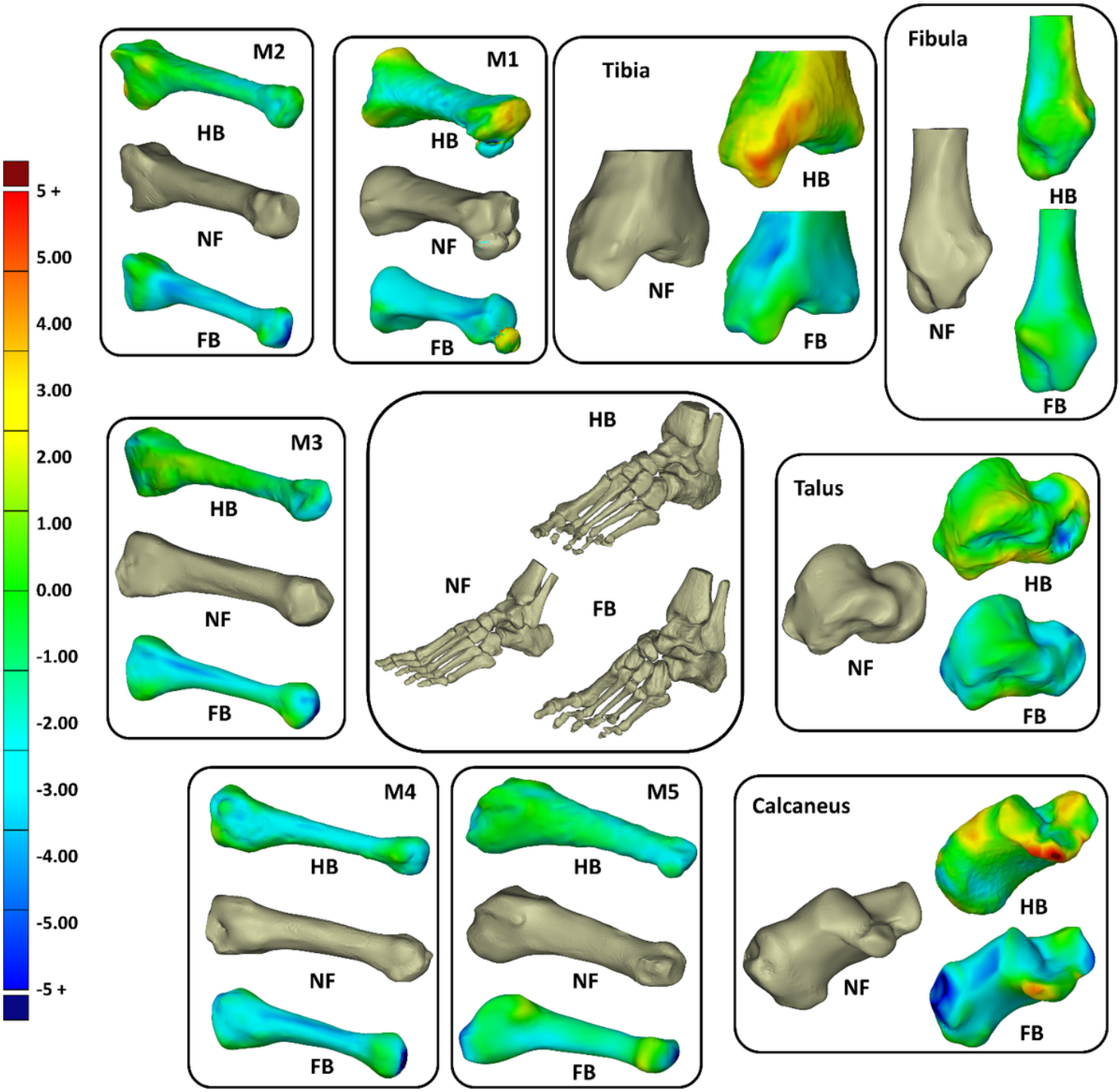

Figure 5

Overall shape comparisons of the calcaneus, talus, tibia, fibular and metatarsal (M1-M5) bones of the NF, HB, and FB foot (consistent colour scale with unit in mm).

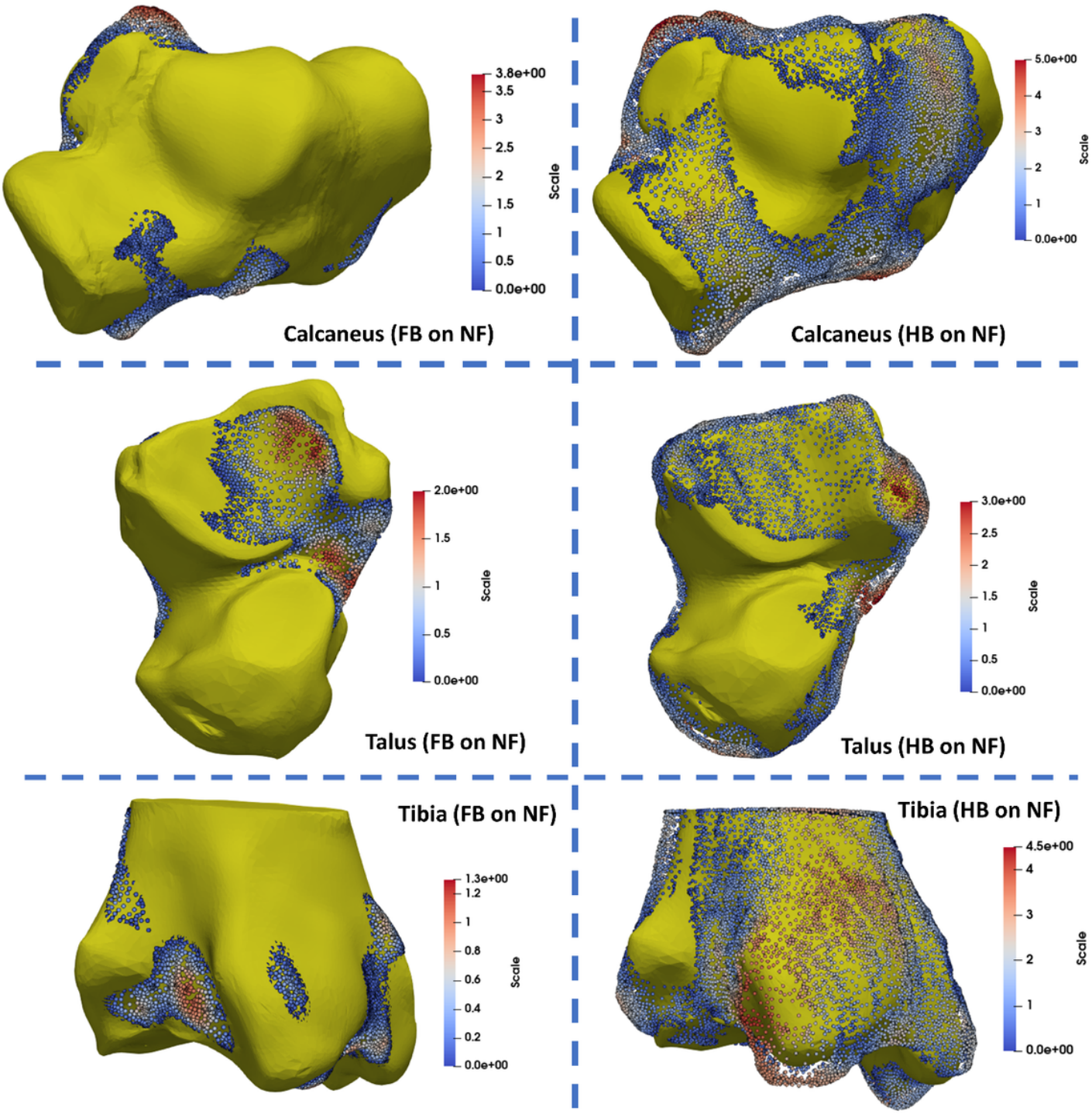

Figure 6

Quantification of Regional Shape Variations in the Calcaneus, Talus and Tibia Bones of the NF, HB, and FB foot (unit in mm).

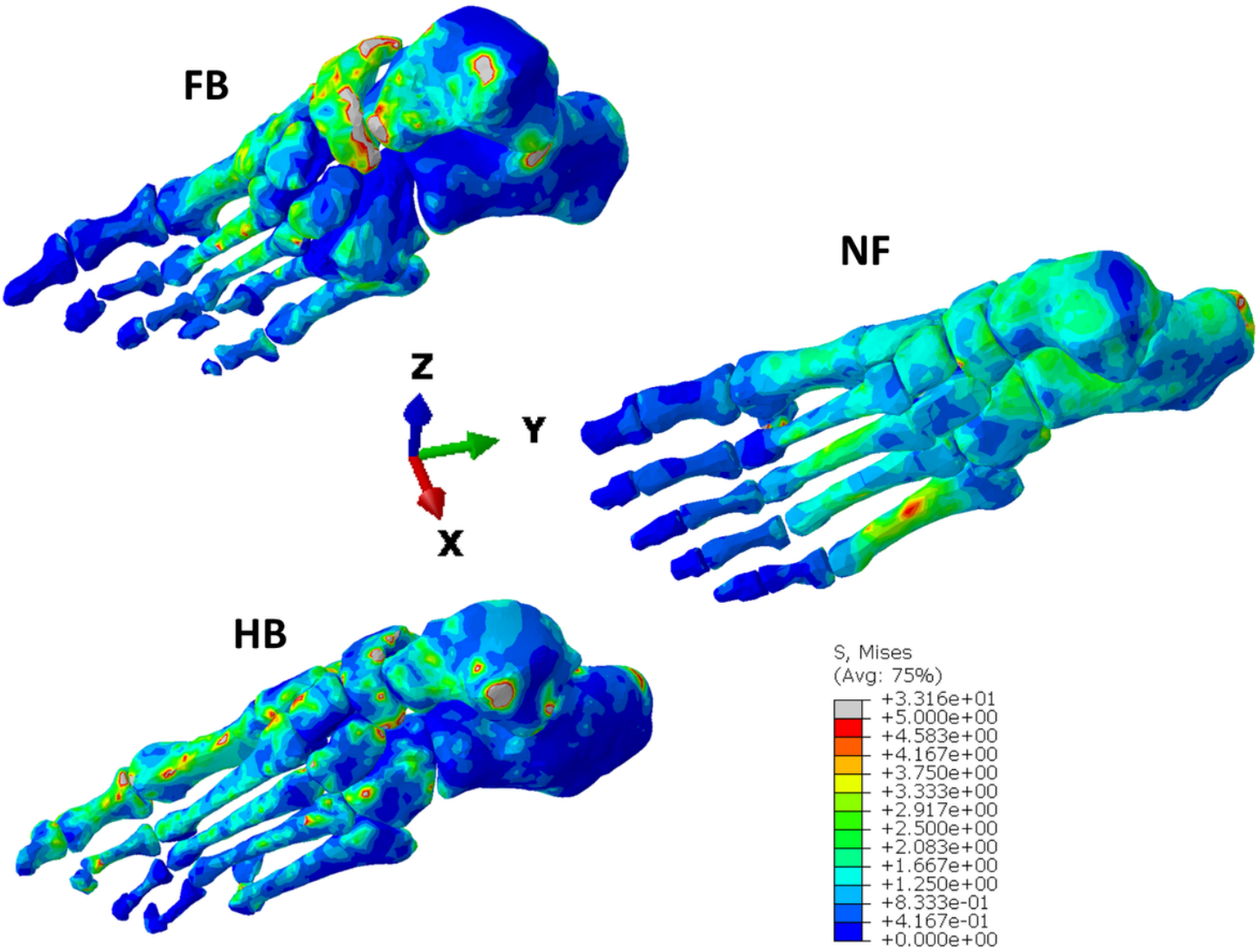

Figure 7

The von Mises stress distribution in the NF, HB and FB foot models

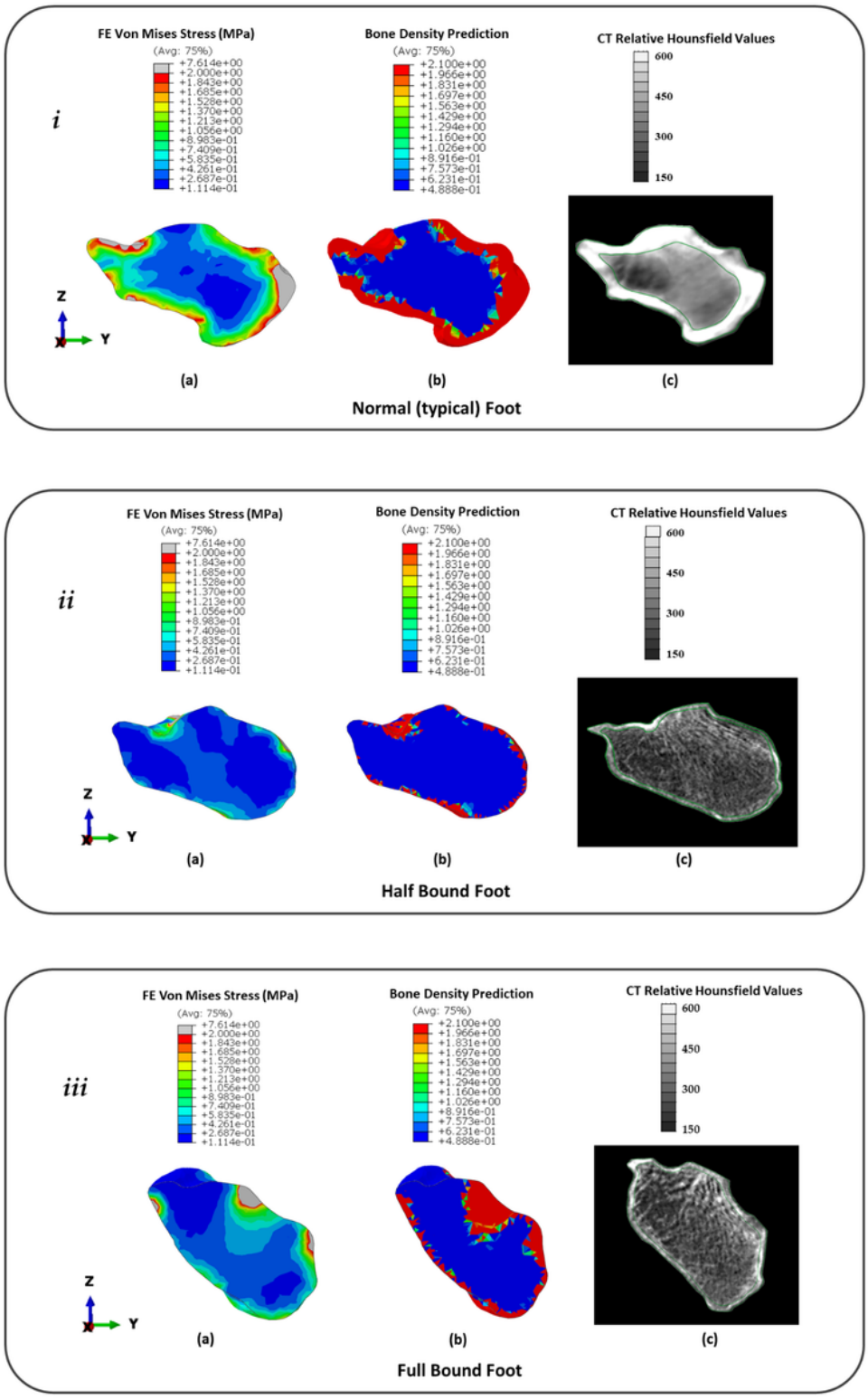

Figure 8

Distribution of FE predicted von Mises (VM) stress (***a***), predicted bone density (g/cm^3) using remodeling algorithm (***b***), and CT with relative Hounsfield units (***c***) for the calcaneus in the typical (normal) NF (***i***), HB (***ii***), and FB (***iii***) foot.

Supplementary Files

This is a list of supplementary files associated with this preprint. Click to download.

- supplementarydocuments.pdf
- appendixA.docx